


First-principle investigation of the charge injection barriers of polyethylene and polytetrafluoroethylene oligomers

Cite as: J. Appl. Phys. **126**, 035101 (2019); <https://doi.org/10.1063/1.5089863>

Submitted: 23 January 2019 . Accepted: 30 May 2019 . Published Online: 15 July 2019

Xi Chen, Aixuan Zhao , Jiaming Li, Junbo Deng , Guanjin Zhang, and Xuefeng Zhao

COLLECTIONS

 This paper was selected as Featured



View Online



Export Citation



CrossMark

ARTICLES YOU MAY BE INTERESTED IN

High performance $\text{In}_{0.83}\text{Ga}_{0.17}\text{As}$ SWIR photodiode passivated by $\text{Al}_2\text{O}_3/\text{SiN}_x$ stacks with low-stress SiN_x films

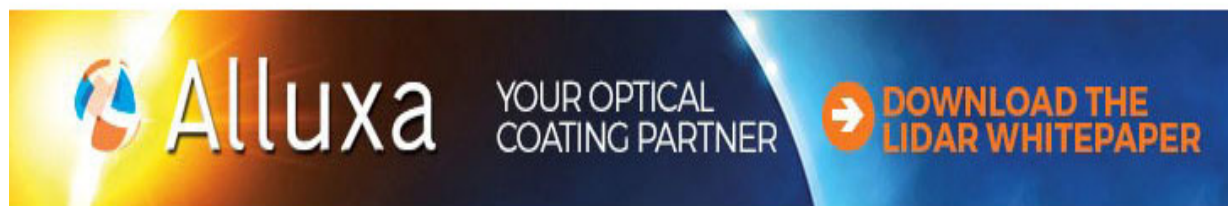
Journal of Applied Physics **126**, 033101 (2019); <https://doi.org/10.1063/1.5090393>

Integrated photonics for low transverse emittance, ultrafast negative electron affinity GaAs photoemitters

Journal of Applied Physics **126**, 033102 (2019); <https://doi.org/10.1063/1.5093938>

Photovoltage-induced blockade of charge and spin diffusion in semiconducting thin films

Journal of Applied Physics **126**, 025701 (2019); <https://doi.org/10.1063/1.5098878>



First-principle investigation of the charge injection barriers of polyethylene and polytetrafluoroethylene oligomers

Cite as: J. Appl. Phys. 126, 035101 (2019); doi: 10.1063/1.5089863

Submitted: 23 January 2019 · Accepted: 30 May 2019 ·

Published Online: 15 July 2019



Xi Chen,¹ Aixuan Zhao,¹ Jiaming Li,¹ Junbo Deng,^{1,a)} Guanjun Zhang,^{1,b)} and Xuefeng Zhao²

AFFILIATIONS

¹State Key Laboratory of Electrical Insulation and Power Equipment, Xi'an Jiaotong University, Xi'an 710049, People's Republic of China

²Electric Power Research Institute of State Grid Shaanxi Electric Power Company, Xi'an 710000, People's Republic of China

^{a)}Email: dengjb@mail.xjtu.edu.cn

^{b)}Email: gjzhang@mail.xjtu.edu.cn

ABSTRACT

Experimental research has shown that much less charge injection occurs in polytetrafluoroethylene (PTFE) compared to polyethylene (PE). To clarify the mechanisms of charge injection from metals into polymer insulators, we comparatively studied charge injection in PE and PTFE oligomers using first-principles calculations. Two different models were studied: chemisorption (bonding) and physisorption (non-bonding). The results show that the electron injection barrier of the metal/PTFE interface is larger than that of the metal/PE interface only in the case of chemisorption. The larger electron injection barrier of the metal/PTFE oligomer interface is mainly affected by the positive vacuum level shift of the metal/PTFE interface induced by electron transfer from the metal to PTFE along the chemical bonds. In the case of physisorption, the hole injection barrier of the metal/PTFE interface is larger than that of the metal/PE interface. This is attributed to the larger ionization potential of PTFE compared to PE. The calculated results reasonably explain the experimental phenomena. The agreement between the experimental and calculated results verifies the rationality of our calculation models. The models used herein can likely be applied in other metal/polymer interfacial systems with acceptable accuracy.

Published under license by AIP Publishing. <https://doi.org/10.1063/1.5089863>

I. INTRODUCTION

Polymers such as polyethylene (PE) and polytetrafluoroethylene (PTFE) have been widely employed as insulation materials in electrical apparatus such as cables and capacitors due to their excellent insulating performance. The aging of cable insulation accelerates under high electric field, which is related to the space charge injected from the metal conductor to the polymer insulator.¹ Space charge can distort the electric field distribution in cables, leading to further acceleration of electrical aging and even insulation failure.² Experimental studies have shown that compared to PE, much less charge is injected into PTFE from the electrode.³ Inspired by this effect, some researchers have fluorinated the surface of PE to improve its insulation performance⁴ and found that surface fluorination greatly decreases the amount of injected charge compared to pure PE.^{5–8} Based on X-ray photoelectron spectroscopy, the surface fluorination process

introduces new functional groups such as $-\text{CF}$, $-\text{CF}_2$, and $-\text{CF}_3$ onto the surface of PE.⁵ These findings suggest that the C–F bonds of both PTFE itself and surface-fluorinated PE at polymer insulator/metal interfaces significantly suppress charge injection. The experimental results mentioned above provide us with a new perspective to understand the nature of charge injection at the interfaces between metals and polymer insulators. However, it remains unclear how C–F bonds influence the charge injection barriers at these interfaces.

Extensive studies have been carried out on semiconductor interfaces^{9–11} and gas adsorption.^{12–16} However, few reports focus on charge injection at the interfaces between metals and polymer insulators. Sato *et al.* comparatively analyzed hole injection at the interfaces of metal/PE and metal/ethylene-vinyl acetate (EVA) copolymer oligomers using first-principles calculations. They found that the molecular dipole moment of EVA oligomer is primarily responsible

for the decreased hole injection barrier at the metal/EVA interface compared to at the metal/PE interface.¹⁷ Chen *et al.* evaluated the charge injection barrier at metal/PE interfaces and concluded that the charge injection barrier is determined by the combined effect of the metal work function and vacuum level shift.¹⁸ Wang *et al.* evaluated the difference in the charge injection barriers of metal/PE and metal/PTFE interfaces from a quantum chemical perspective.³ However, detailed adsorption models explaining the charge injection processes at PE/metal and PTFE/metal interfaces are lacking. To clarify these processes, the charge injection barriers of metal/PE and metal/PTFE interfaces were comparatively studied based on both physical and chemical models using first-principles calculations.

It should be noted that the charge injection barrier of a metal/polymer interface is influenced by multiple factors, including the physical and chemical structures of the metal and polymer along with their interface.¹⁸ However, few experimental data about charge injection barriers are available as reference data for calculations. In this study, we employ density functional theory (DFT) to describe the interfacial properties of PE and PTFE. Considering the complexity of polymer conformations and computational efficiency, C_6H_{14} (PE oligomer) and C_6F_{14} (PTFE oligomer) are adopted to evaluate differences of the charge injection barriers at the respective interfaces from the perspective of quantum mechanics. Since the electronic properties of PE are very close to those computed for linear alkanes (C_nH_{2n+2}) with n of the order of 15–20¹⁹ and smaller alkanes such as C_7H_{16} ¹⁷ and C_9H_{20} ¹⁸ were usually utilized in the interfacial problems, this simplification is reasonable.

This paper first describes the models applied in the calculations. Next, we briefly introduce the energy level theory utilized to calculate the charge injection barrier and a series of parameters including metal work functions, electron affinity, and ionization potential. These parameters are compared to experimental values and then used to calculate the charge injection barriers. Finally, we comparatively analyze the charge injection barriers at the metal/PE and metal/PTFE interfaces.

II. MODELS

The metal/PE and metal/PTFE interfaces were constructed by placing C_6H_{14} and C_6F_{14} molecules, respectively, on an asymmetric metal slab. The top of the metal slab was covered by adsorbed molecules. Each unit cell was composed of a metal slab with six atomic layers, an adsorbed molecule, and a vacuum layer (no less than 16 Å). Two types of models were applied: a bonding model and a nonbonding model in which the adsorbed molecules were parallel and perpendicular to the metal surface, respectively (Fig. 1). In Fig. 1(a), the oligomer (i.e., C_6H_{13} free radical) forms chemical bonds with metal atoms. In contrast, in Fig. 1(b), the C_6H_{14} molecule does not. For convenience, we refer to the bonding model as chemisorption and the nonbonding model as physisorption in the remainder of this paper. The Cu(100) and Al(100) metal surfaces were selected since they are the most widely used conductors in electrical apparatus and have been previously studied experimentally.^{3,20}

III. ENERGY LEVEL ALIGNMENT AT INTERFACES

Before the polymer and metal surface come into contact with each other, they share the same vacuum level. When a polymer

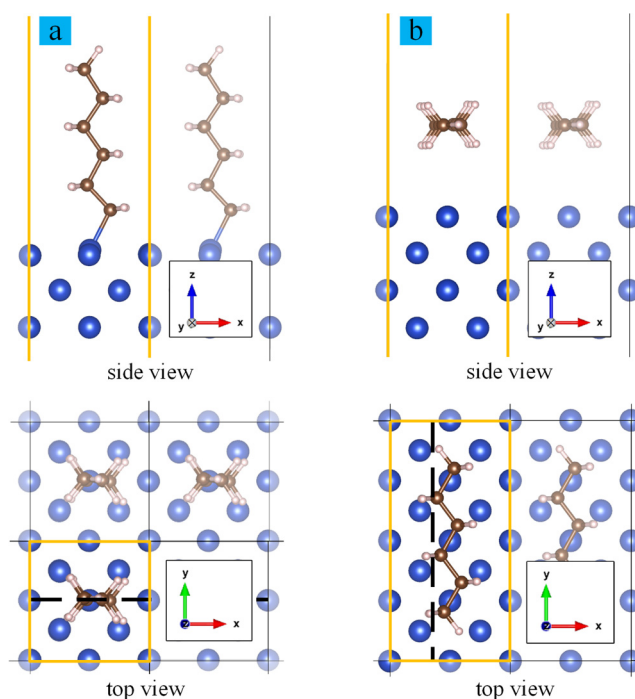


FIG. 1. Interfacial models of polyethylene oligomer (C_6H_{13} and C_6H_{14}) adsorbed on the Cu(100) surface via (a) chemisorption and (b) physisorption. The dashed lines denote the cross sections where the electron density was evaluated (see also Fig. 5). Hydrogen, carbon, and copper atoms are colored in light brown, brown, and blue, respectively. The solid yellow frames indicate the unit cell. The models are displayed using VESTA,²¹ a structural model visualization package.

contacts a metal surface, the unaligned Fermi levels of the metal and polymer create a dipole moment, resulting in a shift in the vacuum level at the interface ($\Delta\phi$),²² as shown in Fig. 2. Therefore, the electron injection barrier ϕ_e and the hole injection barrier ϕ_h can be, respectively, expressed as

$$\phi_e = \psi_m - \text{VEA} + \Delta\phi \quad (1)$$

and

$$\phi_h = -\psi_m + \text{VIP} - \Delta\phi, \quad (2)$$

where VEA and VIP are the vertical electron affinity and vertical ionization potential, respectively, and ψ_m is the metal work function. The vacuum level shift $\Delta\phi$ has been extensively studied in previous works.^{23–25} Since VEA and VIP are computed under vacuum in an isolated state, the image potential effect²⁶ is not taken into account in this study.

The GW method, which is based on many-body perturbation theory, is the state-of-the-art approach for treating VIP and VEA. Thus, the GW method was applied in this study to compute the VIP and VEA for both PE and PTFE oligomers. VIP and VEA can

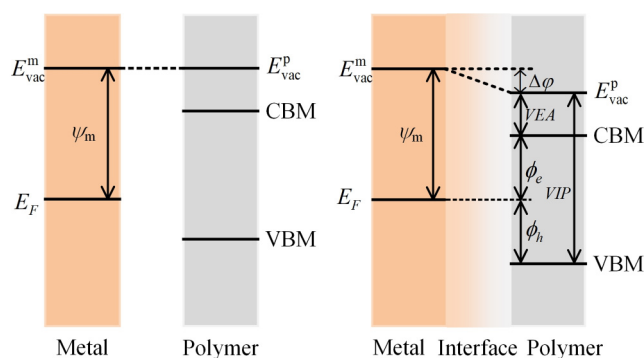


FIG. 2. Energy levels of metal and polymer before (left) and after (right) coming into contact with each other. CBM, VBM, and E_F are the conduction band maximum, the valence band minimum, and the Fermi energy, respectively. E_{vac}^m and E_{vac}^p are the vacuum levels of the metal and polymer, respectively. The sign of the vacuum level shift ($\Delta\phi$) is negative.

be expressed as

$$VIP = E_{vac} - E_{HOMO}^{QP} \quad (3)$$

and

$$VEA = E_{vac} - E_{LUMO}^{QP}, \quad (4)$$

where E_{vac} is the vacuum level calculated from the planar-averaged electrostatic potential at the DFT level of theory and E_{HOMO}^{QP} and E_{LUMO}^{QP} denote the quasiparticle energies corresponding to highest occupied molecular orbital (HOMO) and lowest unoccupied molecular orbital (LUMO), respectively.²⁷

The work function of a metal is defined as the energy difference between its Fermi level and vacuum level. The most widely used method to compute metal work function is the “bulk plus band lineup” method.²⁸ In this method, the bulk model is introduced to correct the Fermi energy calculation error generated by slab calculation. However, in our calculations, the thickness of the six atomic metal layers was sufficient for the computed results to converge well as the number of atomic metal layers increased; thus, we did not consider the bulk correction. Figure 3 shows the planar-averaged electrostatic potentials of physically adsorbed PE and PTFE oligomers on the Cu(100) surface. The vacuum level shift ($\Delta\phi$), metal work function, and Fermi level are labeled within Fig. 3.

IV. COMPUTATIONAL DETAILS

All calculations were carried out within the DFT framework in the Quantum Espresso (pwscf) code,²⁹ which incorporates ultrasoft pseudopotentials. Electric structure and geometry optimizations were carried out using the generalized gradient approximation (GGA) Perdew–Burke–Ernzerhof (PBE)³⁰ functional exchange–correlation energies. The kinetic energy cutoff was at least 30 Ry for wavefunctions. Weak interactions, including van der Waals forces, which are important in physisorption, were described with the DFT-D3

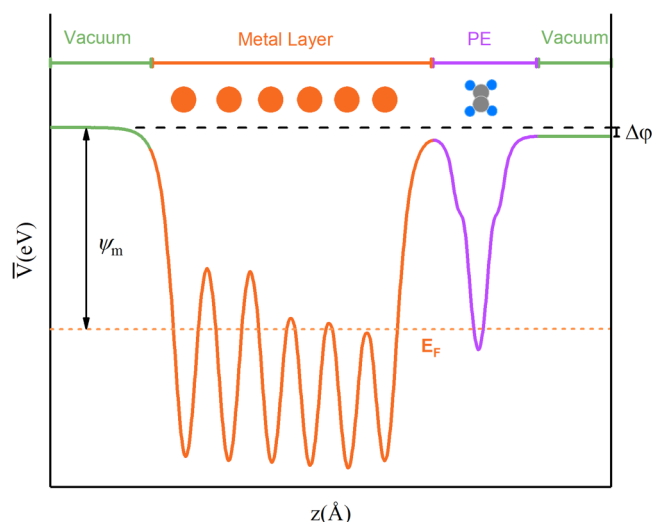


FIG. 3. Planar-averaged electrostatic potentials (\bar{V}) of physically adsorbed PE and PTFE oligomers on the Cu(100) surface. The horizontal axis denotes the z-axis coordinate of the built models.

functional.³¹ All atomic coordinates were relaxed until the force of each atom was less than 0.0514 eV/Å. Surface dipole correction was applied within the area of the vacuum layer to handle the asymmetric nature of the heterojunction.³² The coordinate relaxation and properties for bulk metal, isolated molecules, and interfaces were calculated using $3 \times 3 \times 3$, $1 \times 1 \times 1$, and $4 \times 2 \times 1/4 \times 4 \times 1$ (physisorption/chemisorption) Monkhorst–Pack meshes, respectively, to sample the first Brillouin zone. The VIP and VEA of isolated molecules were calculated using the G_0W_0 approximation implemented in West code³³ after the DFT calculation.

V. RESULTS AND DISCUSSION

A. Lattice constants and metal work functions

The computed lattice constants are shown in Table I. The calculated lattice constant of Cu is 3.62 Å, which agrees with the experimental value of 3.61 Å. The six-atomic-layer metal slab models were cleaved from the relaxed bulk structures. The initial slab structures were then subsequently relaxed with the bottom three layers fixed to mimic bulk behavior. The computed metal

TABLE I. Comparison of calculated and experimental lattice constants and work functions.

Metal surface	Calculated lattice constant (Å)	Experimental lattice constant (Å)	Calculated work function (eV)	Experimental work function (eV)
Cu(100)	3.62	3.61 ³⁴	4.57	4.59 ³⁵
Al(100)	4.05	4.05 ³⁴	4.16	4.20 ³⁶

work functions are also shown in Table I. All computed results are within 6% of the corresponding experimental data, indicating that the computational method adopted in this paper is valid and effective for determining metal work functions. The computed values shown in Table I were utilized in subsequent calculations.

B. Electron affinity and ionization potential

When calculating the properties of isolated molecules, we adopted the G_0W_0 approximation to obtain the quasiparticle energies of the molecules. VIP and VEA were computed according to Eqs. (3) and (4), respectively. The calculated VIP of C_6H_{14} is 10.41 eV, which agrees well with the experimental value of 10.03 ± 0.15 eV.³⁷ The computed VEAs of C_6H_{14} and C_6F_{14} calculated using the G_0W_0 approximation are -0.87 and -1.17 eV, respectively. However, the LUMO of PE oligomer is a Rydberg-like state,¹⁷ whereas bulk PE has “interchain” character.³⁸ Thus, the electron affinity of a single PE oligomer might differ from that of bulk PE. The electron affinities of bulk PE with chains perpendicular and parallel to the surface normal were calculated to be -0.17 and -0.10 eV, respectively;³⁹ thus, these values were applied to evaluate the physisorption and chemisorption of PE in this study. For PTFE oligomers, VEA has the opposite sign as the adiabatic electron affinity (AEA),⁴⁰ indicating that the exact electron affinity of PTFE oligomer is poorly described by VEA. The AEA of C_6F_{14} , which is more precise and reflective of the actual situation compared to VEA, was calculated to be 0.69 eV using the hybrid functional B3LYP.⁴⁰ Thus, this value was utilized herein.

Since no experimental ionization potential of C_6F_{14} was available, we performed calculations for a series of fluorocarbons (CF_4 , C_2F_6 , and C_3F_8) to evaluate the precision of Eq. (3) for determining the VIP of C_6F_{14} . The experimental ionization potentials of CF_4 , C_2F_6 , and C_3F_8 are 16.2,⁴¹ 13.6–14.4,⁴² and 13.38 eV,⁴³ respectively, while the corresponding calculated values are 15.25, 13.64, and 13.03 eV, respectively. The experimental and calculated values show good agreement and indicate a decreasing trend in ionization potential with increasing number of carbon atoms. The computed ionization potential of C_6F_{14} is 11.45 eV. Given the lack of experimental ionization potential data for C_6F_{14} , we adopted this calculated value in subsequent calculations based on the acceptable errors in the calculated ionization potentials of the other fluorocarbons.

C. Charge injection barrier

The structures of the metal/PE and metal/PTFE interfaces were formed by placing PE and PTFE molecules that were optimized under vacuum on a metal slab and allowing the molecules and the top two metal layers to relax. The adsorption of the PE and PTFE molecules on the metal surface causes a change in dipole moment and hence a shift in vacuum level (Figs. 2 and 3). Although PE, PTFE, and their oligomers have no permanent dipole moment, the interactions between the metal surface and adsorbed molecules (e.g., the image force effect⁴⁴ and Pauli repulsion⁴⁵) cause electron redistribution and hence induce a dipole moment. The computed vacuum level shift is shown in Table II. In most cases, $\Delta\phi$ is negative due to the movement of electrons from PE or PTFE to the metal. Only the $\Delta\phi$ of the metal/PTFE oligomer (chemisorption) interfaces has large positive values. The positive

TABLE II. Vacuum level shift (eV).

	Physisorption		Chemisorption	
	PE	PTFE	PE	PTFE
Cu	−0.31	−0.19	−0.61	1.70
Al	−0.09	−0.19	−0.31	1.25

$\Delta\phi$ occurs when metal–carbon bonds form, facilitating spontaneous charge transfer which might originate from the strong electronegativity of fluorine and the positive electron affinity of PTFE.

The projected density of states (PDOS) curves for C_6H_{14} and C_6F_{14} adsorbed onto Cu(100) are shown in Fig. 4. Since the Projwfc code (part of pwscf) uses only atomic (pseudo-) orbitals contained in the pseudopotential files, the PDOS curves do not include some peaks above the Fermi level. For C_6H_{14} , the PDOS curve for chemisorption [red curve in Fig. 4(a)] shifts left compared to the curve corresponding to physical adsorption [black curve in Fig. 4(a)]. In contrast, the opposite trend is observed in the PDOS curves of C_6F_{14} , indicating a higher electron injection barrier. This result is in agreement with the signs of the vacuum level shifts in Table II.

To investigate charge transfer during adsorption, we visualized the difference charge distributions of the Cu(100)/PE and Cu(100)/PTFE heterojunction systems before and after adsorption (Fig. 5). The difference charge distribution of a heterojunction can be defined as

$$\rho_{\text{diff}} = \rho_{\text{Cu/(PE/PTFE)}} - \rho_{\text{PE/PTFE}} - \rho_{\text{Cu}}, \quad (5)$$

where $\rho_{\text{Cu/(PE/PTFE)}}$ is the charge density of the whole adsorption system, $\rho_{\text{PE/PTFE}}$ is the charge density of the single adsorbed oligomer and ρ_{Cu} is the charge density of single Cu substrate. After

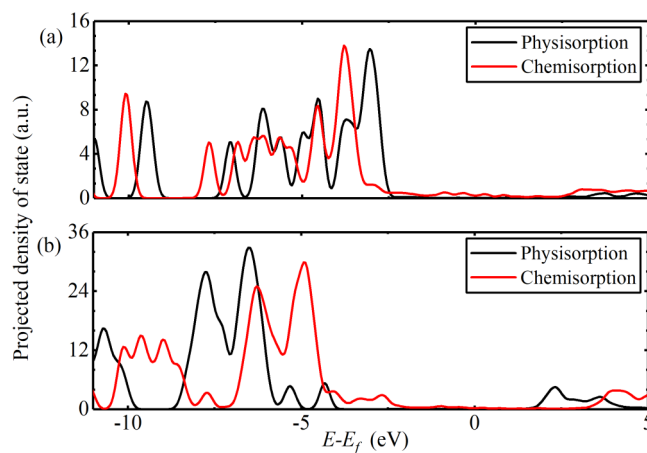


FIG. 4. PDOS curves of (a) PE oligomer and (b) PTFE oligomer adsorbed physically (black curves) and chemically (red curves) onto Cu(100) slabs with a Gaussian broadening energy of 0.2 eV.

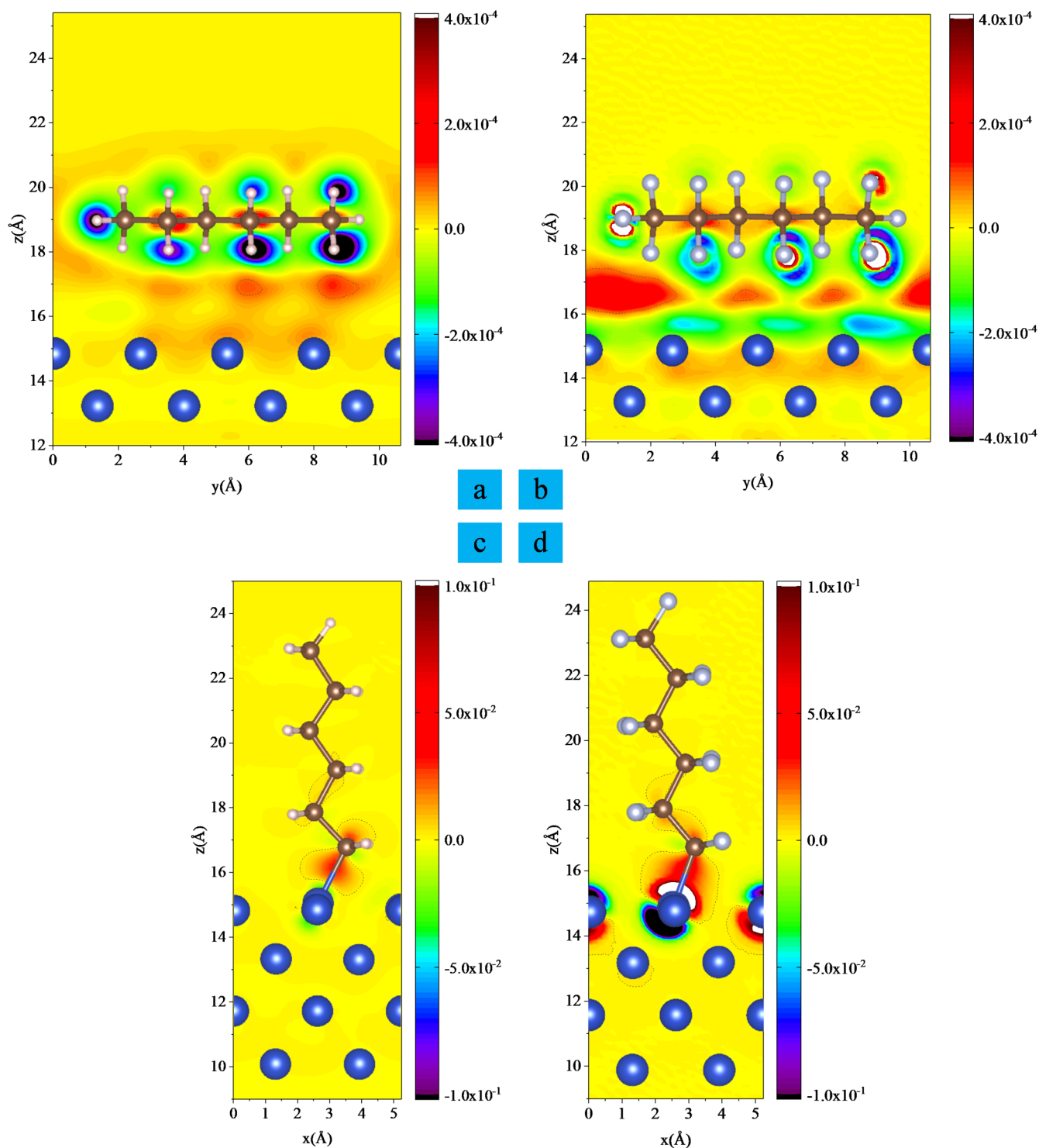


FIG. 5. Difference charge distributions along the cross sections indicated in Fig. 1 before and after the adsorption of PE and PTFE oligomers on the Cu(100) surface. The dashed contour lines in (a) and (b) denote a difference in electron density of 8×10^{-5} , while those in (c) and (d) indicate a difference of 2×10^{-3} . The white and black areas denote differences in electron density that are outside the range of the color scale bar. The units of electron density difference are e/bohr^3 .

physisorption, the charge density changed the most around H and F atoms; thus, the charge density is shown along the cross section close to these atoms rather than close to carbon atoms (see also Fig. 1). The distributions of the difference in charge density for physically adsorbed PE [Fig. 5(a)] and PTFE [Fig. 5(b)] molecules show some similarities. Upon adsorption, electrons transfer from the molecules and the metal surface to the area between them, consistent with previous reports.¹⁷ However, some key differences are observed. Electron accumulation in the area between the C₆F₁₄ molecule and the Cu(100) surface is more significant than that between the C₆H₁₄ molecule and the Cu(100) surface. In addition, the hydrogen atoms in C₆H₁₄ lose a large amount of electrons [black areas in Fig. 5(a)], whereas the fluorine atoms in C₆F₁₄ attract many electrons [white areas in Fig. 5(b)]. For chemical adsorption, the redistribution of charge density in the Cu(100)/PTFE structure is much more significant and complex than in the Cu(100)/PE structure. This might be attributed to the strong electronegativity of the fluorine atoms. A large amount of electrons move spontaneously from the metal surface to the PTFE molecule along the metal-carbon bonds. Thus, the chemical bonds between the metal slab and carbon atoms work like bridges to facilitate charge transfer. These results indicate that charge transfer has a large effect on the vacuum level shift and hence the charge injection barrier.

The adsorption energies (E_{ad}) of PE and PTFE on the Cu(100) and Al(100) surfaces (Table III) were calculated according to the following equation:

$$E_{ad} = E_{\text{Metal/Oligomer}} - E_{\text{Metal}} - E_{\text{Oligomer}}, \quad (6)$$

where $E_{\text{Metal/Oligomer}}$ is the total energy of the metal/PE or metal/PTFE interfacial structure, E_{Metal} is the total energy of the metal slab, and E_{Oligomer} is the total energy of the PE or PTFE oligomer. In the case of chemisorption, E_{Oligomer} in Eq. (6) is replaced with the energy of C₆H₁₃ or C₆F₁₃ radical. Since the adsorption area of physisorption is much larger than that of chemisorption, the physisorption energies shown in Table IV are the averaged values of each CH₂ or CF₂ structure ignoring the terminal H or F atoms of the PE or PTFE oligomer. All the computed adsorption energies are negative, indicating that the adsorptions of both PE and PTFE on the metal slab are energetically favorable. The adsorption energies of the metal/PTFE interfaces are more negative than those of the metal/PE interfaces, indicating that the adsorption of PTFE is more energetically favorable than that of PE.

Table IV shows the computed charge injection barriers, including both electrons and holes, from the Cu(100) and Al(100) surfaces to the PE and PTFE oligomers for both physisorption and

TABLE IV. Charge injection barriers (eV).

		Physisorption		Chemisorption	
		PE	PTFE	PE	PTFE
Cu(100)	φ_e	4.43	3.69	4.06	5.57
	φ_h	6.15	7.07	6.45	5.18
Al(100)	φ_e	4.24	3.27	3.95	4.72
	φ_h	6.34	7.48	6.56	6.04

chemisorption. In an experiment, both holes and electrons injected into PTFE are much less than PE. While it is impossible to experimentally control the type of adsorption (physisorption vs chemisorption), we provide two sets of results for physisorption and chemisorption from a computational and theoretical perspective.

The barriers to electron injection at the Cu(100)/PTFE interface are 3.69 and 5.57 eV for physisorption and chemisorption, respectively, while those for the Cu(100)/PE interface are 4.43 and 4.06 eV, respectively. Considering Eq. (1) and previous analyses, we can conclude that the huge increase of electron injection barrier at Cu(100)/PTFE interface from physisorption to chemisorption is dominated by the vacuum level shift induced by charge transfer. At the metal/PTFE interface, the formation of metal-carbon bonds facilitates electron transfer, resulting in a positive larger vacuum level shift and a larger induced dipole moment compared to the metal/PE heterojunction, which ultimately leads to an increase in the electron injection barrier. In other words, the original spontaneous charge transfer into PTFE oligomers makes further electron injection more difficult, unlike at metal/PE interfaces. This condition is most likely to occur in locations with abundant electrons such as cathodes.

In contrast, the hole injection barrier of the metal/PTFE heterojunction is larger than that of the metal/PE interface only in the case of physisorption. It should be noted here that the anode/polymer interface is usually positively charged. This means that the charge transfer-induced positive vacuum level shift and the dipole layer are destroyed by the external opposite potential bias. The hole injection barrier of the Cu/PTFE interface for physisorption is 7.07 eV, approximately 1 eV larger than that of the Cu/PE interface (6.15 eV). Similar results were obtained for the Al/PE and Al/PTFE interfaces. According to Eq. (2), the larger hole injection barrier of PTFE compared to PE primarily originates from the larger ionization potential of PTFE, which likely results from the strong electronegativity of fluorine.

To evaluate the charge injection process, we visualized the differences in plane-averaged electron density before and after an external electric field was applied to the system. In the case of physisorption, the oligomers do not have any connection with the metal surface, and the charge transfer process is not visible under an electric field. Therefore, an electric field was applied to the chemisorption models to visualize the electron redistribution along with the amount of electrons injected into the oligomers. The difference in plane-averaged electron density was calculated using the effective screening method (ESM).⁴⁶ A semi-infinite medium with relative permittivity $\epsilon_r = 1$ (i.e., the vacuum) was set at the left side, while a metal medium with $\epsilon_r = \infty$ was set at the right side, as shown in

TABLE III. Adsorption energies (eV).

	Physisorption/ (CH ₂ or CF ₂)		Chemisorption	
	PE	PTFE	PE	PTFE
Cu(100)	-0.17	-0.26	-2.21	-2.60
Al(100)	-0.08	-0.36	-2.11	-3.38

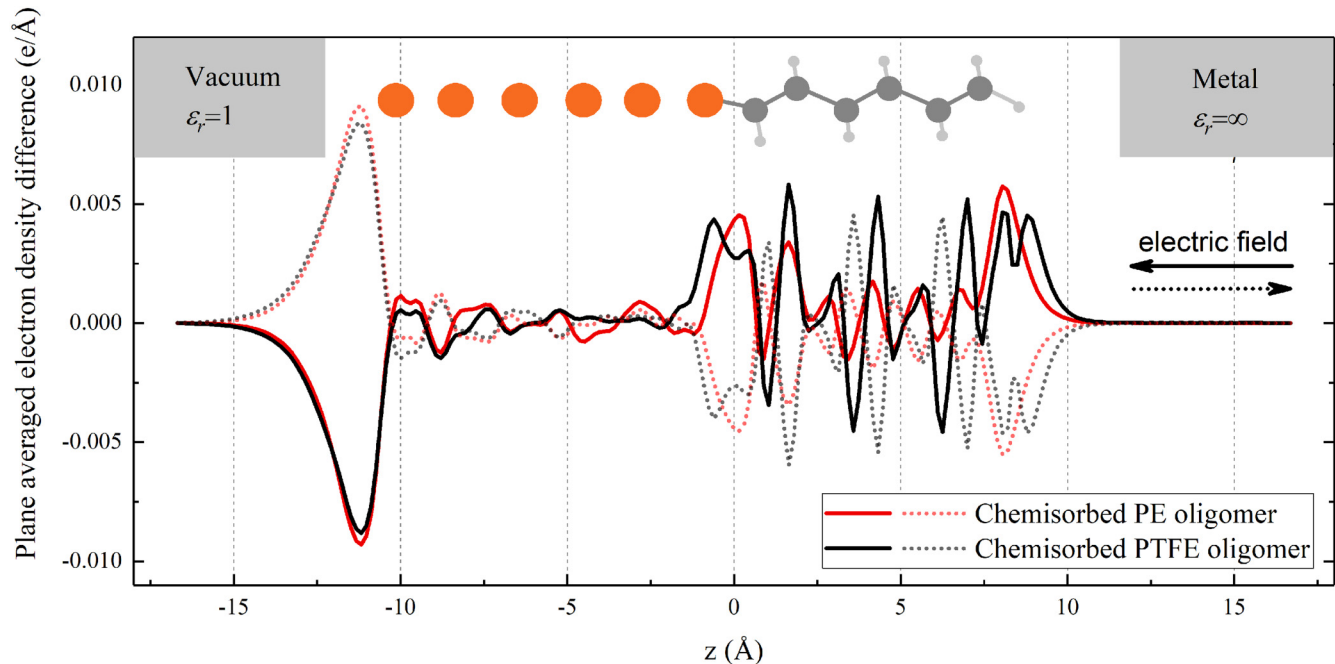


FIG. 6. Differences in plane-averaged electron density along the z -axis for chemisorbed PE and PTFE oligomers. The gray areas denote the locations of the effective media of vacuum and metal. An electric field of 0.002 Ry/a.u. was applied along the z -axis. A single orange ball denotes the location of a layer of Cu atoms. The dark-gray and light-gray balls denote the approximate positions of the PE and PTFE oligomers, respectively.

Fig. 6. A finite electric field of 0.002 Ry/a.u. was applied to the model to visualize the electron redistribution. The curves in **Fig. 6** show the differences in plane-averaged electron density of the interfaces with oligomers chemisorbed on the Cu(100) surface along the z -axis. The coordinates of the entire model were adjusted so that the Cu–C bond was located at point 0 on the z -axis. When the electric field is applied along the negative direction of the z -axis, the electrons lost by the metal primarily accumulate at the interface (Cu–C bond) and the oligomers' right side. The integrated values of the solid lines (dashed lines) from 0 to 15 along the z -axis are 0.01278 and 0.01188 e (−0.01293 and −0.01193 e) for PE and PTFE oligomers, respectively. Thus, fewer electrons and holes are injected into the PTFE oligomer than into the PE oligomer. This result is qualitatively consistent with both the calculated and experimental findings.

VI. CONCLUSION

The charge injection barriers of metal/PE and metal/PTFE interfaces were evaluated using first-principles calculations. The results indicate that the electron injection barrier of the metal/PTFE interface is larger than that of the metal/PE interface only in the case of chemisorption, while the hole injection barrier of the metal/PTFE interface exceeds that of the metal/PE interface only in the case of physisorption. In places where electrons are dominant, spontaneous electron transfer from the metal side to the PTFE side becomes possible, increasing the vacuum level shift and hindering further electron

injection. The larger hole injection barrier of the metal/PTFE interface compared to the metal/PE interface is attributed to the larger ionization potential of PTFE compared to PE, which presumably results from the strong electronegativity of fluorine.

ACKNOWLEDGMENTS

Constructive discussions with Dr. Qu Guanghao are gratefully acknowledged. This work was supported by the National Natural Science Foundation of China (NNSFC) (Nos. 51577150 and 11775175) and the Key Research and Development Program of Shaanxi Province (No. 2018GY-001).

REFERENCES

- ¹G. Chen, M. Fu, X. Liu, and L. Zhong, *J. Appl. Phys.* **97**, 083713 (2005).
- ²K. Wu, Y. Wang, X. Wang, M. Fu, and S. Hou, *IEEE Electr. Insul. Mag.* **33**, 53 (2017).
- ³W. Wang, T. Takada, Y. Tanaka, and S. Li, *IEEE Trans. Dielectr. Electr. Insul.* **24**, 2599 (2017).
- ⁴A. Zhao, X. Chen, S. Chen, C. Yao, X. Zhao, J. Deng, and G. Zhang, *AIP Adv.* **9**, 015102 (2019).
- ⁵N. Liu, Z. Li, G. Chen, Q. Chen, and S. Li, *Mater. Res. Express* **4**, 075308 (2017).
- ⁶K. Takashima and T. Oda, *Ind. Appl. IEEE Trans.* **36**, 76 (2000).
- ⁷Z. An, Q. Yang, C. Xie, Y. Jiang, F. Zheng, and Y. Zhang, *J. Appl. Phys.* **105**, 064102 (2009).
- ⁸Z. An, C. Xie, Y. Jiang, F. Zheng, and Y. Zhang, *J. Appl. Phys.* **106**, 104112 (2009).

- ⁹T. Toda, J.-I. Hanna, and T. Tani, *J. Appl. Phys.* **101**, 024505 (2007).
- ¹⁰N. Ghaderi, S. J. Hashemifar, H. Akbarzadeh, and M. Peressi, *J. Appl. Phys.* **102**, 074306 (2007).
- ¹¹R. Cao, Z. Zhang, C. Wang, H. Li, X. Xie, H. Dong, H. Liu, and W. Wang, *J. Appl. Phys.* **117**, 135302 (2015).
- ¹²P. S. Bagus, K. Hermann, and C. Woll, *J. Chem. Phys.* **123**, 184109 (2005).
- ¹³Y. Morikawa, H. Ishii, and K. Seki, *Phys. Rev. B* **69**, 041403(R) (2004).
- ¹⁴P. C. Rusu and G. Brocks, *J. Phys. Chem. B* **110**, 22628 (2006).
- ¹⁵Y. Cardona Quintero, H. Zhu, and R. Ramprasad, *J. Mater. Sci.* **48**, 2277 (2013).
- ¹⁶H. Cui, X. Zhang, D. Chen, and J. Tang, *Appl. Surf. Sci.* **447**, 594 (2018).
- ¹⁷M. Sato, A. Kumada, and K. Hidaka, *IEEE Trans. Dielectr. Electr. Insul.* **24**, 574 (2017).
- ¹⁸L. Chen, T. D. Huan, Y. C. Quintero, and R. Ramprasad, *J. Mater. Sci.* **51**, 506 (2016).
- ¹⁹J. J. Pireaux, S. Svensson, E. Basilier, P. Malmqvist, U. Gelius, R. Caudano, and K. Siegbahn, *Phys. Rev. A* **14**, 2133 (1976).
- ²⁰T. Takada, H. Kikuchi, H. Miyake, Y. Tanaka, M. Yoshida, and Y. Hayase, *IEEE Trans. Dielectr. Electr. Insul.* **22**, 1240 (2015).
- ²¹K. Momma and F. Izumi, *J. Appl. Crystallogr.* **44**, 1272 (2011).
- ²²H. Ishii, K. Sugiyama, E. Ito, and K. Seki, *Adv. Mater.* **11**, 605 (1999).
- ²³Y. Morikawa, K. Toyoda, I. Hamada, S. Yanagisawa, and K. Lee, *Curr. Appl. Phys.* **12**, S2 (2012).
- ²⁴Y. Nakano, S. Yanagisawa, I. Hamada, and Y. Morikawa, *Surf. Interface Anal.* **40**, 1059 (2008).
- ²⁵K. Toyoda, I. Hamada, K. Lee, S. Yanagisawa, and Y. Morikawa, *J. Chem. Phys.* **132**, 134703 (2010).
- ²⁶F. Flores, J. Ortega, and H. Vázquez, *Phys. Chem. Chem. Phys.* **11**, 8658 (2009).
- ²⁷M. Govoni and G. Galli, *J. Chem. Theory Comput.* **14**, 1895 (2018).
- ²⁸C. G. Van de Walle and R. M. Martin, *Phys. Rev. B* **35**, 8154 (1987).
- ²⁹P. Giannozzi, S. Baroni, N. Bonini, M. Calandra, R. Car, C. Cavazzoni, D. Ceresoli, G. L. Chiarotti, M. Cococcioni, I. Dabo, A. D. Corso, S. de Gironcoli, S. Fabris, G. Fratesi, R. Gebauer, U. Gerstmann, C. Gougousis, A. Kokalj, M. Lazzeri, L. Martin-Samos, N. Marzari, F. Mauri, R. Mazzarello, S. Paolini, A. Pasquarello, L. Paulatto, C. Sbraccia, S. Scandolo, G. Sclauzero, A. P. Seitsonen, A. Smogunov, P. Umari, and R. M. Wentzcovitch, *J. Phys. Condens. Matter* **21**, 395502 (2009).
- ³⁰J. P. Perdew, K. Burke, and M. Ernzerhof, *Phys. Rev. Lett.* **78**, 1396 (1996).
- ³¹S. Grimme, J. Antony, S. Ehrlich, and H. Krieg, *J. Chem. Phys.* **132**, 154104 (2010).
- ³²L. Bengtsson, *Phys. Rev. B* **59**, 12301 (1999).
- ³³M. Govoni and G. Galli, *J. Chem. Theory Comput.* **11**, 2680 (2015).
- ³⁴C. Kittel, *Introduction to Solid State Physics*, 8th ed. (Wiley, New York, 2005), p. 20.
- ³⁵H. B. Michaelson, *J. Appl. Phys.* **48**, 4729 (1977).
- ³⁶D. R. Lide, *CRC Handbook of Chemistry and Physics* (CRC Press, Boca Raton, 2005).
- ³⁷M. Meot-Ner, L. W. Sieck, and P. Ausloos, *J. Am. Chem. Soc.* **103**, 5342 (1981).
- ³⁸S. Serra, E. Tosatti, S. Iarlari, S. Scandolo, and G. E. Santoro, *Phys. Rev. B* **62**, 4389 (2000).
- ³⁹M. C. Righi, S. Scandolo, S. Serra, S. Iarlari, E. Tosatti, and G. Santoro, *Phys. Rev. Lett.* **87**, 076802 (2001).
- ⁴⁰P. Ankan, Ph.D. thesis, University of Georgia, Athens, 2005.
- ⁴¹T. A. Carlson, A. Fahlman, W. A. Svensson, M. O. Krause, T. A. Whitley, F. A. Grimm, M. N. Piancastelli, and J. W. Taylor, *J. Chem. Phys.* **81**, 3828 (1984).
- ⁴²M. G. Inghram, G. R. Hanson, and R. Stockbauer, *Int. J. Mass Spectrom. Ion Phys.* **33**, 253 (1980).
- ⁴³M. J. S. Dewar and S. D. Worley, *J. Chem. Phys.* **50**, 654 (1969).
- ⁴⁴N. Lang, *Phys. Rev. Lett.* **46**, 842 (1981).
- ⁴⁵P. S. Bagus, V. Staemmler, and C. Wöll, *Phys. Rev. Lett.* **89**, 096104 (2002).
- ⁴⁶M. Otani and O. Sugino, *Phys. Rev. B* **73**, 115407 (2006).